Mathematical Modelling and Control

https://www.aimspress.com/journal/mmc

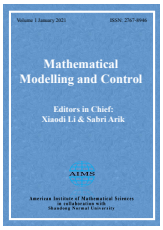

MMC, 4(2): 208–229.
DOI: 10.3934/mmc.2024018
Received: 26 November 2023
Revised: 04 March 2024
Accepted: 05 March 2024
Published: 23 May 2024

Research article

Dynamical analysis of COVID-19 and tuberculosis co-infection using mathematical modelling approach

J. O. Akanni[1,2], S. Ajao[3], S. F. Abimbade[4] and Fatmawati[2,*]

[1] Department of Mathematical and Computing Sciences, Koladaisi University, Ibadan, Oyo State, Nigeria

[2] Department of Mathematics, Faculty of Science and Technology, Universitas Airlangga, Surabaya, Indonesia

[3] Department of Mathematics and Computer Science, Elizade University, Ondo State, Nigeria

[4] Department of Pure and Applied Mathematics, Ladoke Akintola University of Technology, Ogbomoso, Oyo State, Nigeria

* **Correspondence:** Email: fatmawati@fst.unair.ac.id.

Abstract: Both tuberculosis (TB) and COVID-19 are infectious diseases with similar clinical manifestations, which mainly affect the lungs. Clinical studies have revealed that the immunosuppressive drugs taken by COVID-19 patients can affect the immunological functions in the body, which can cause the patients to contract active TB via a new infection or reinfection, and the co-infection of the two diseases portends a clinical complexity in the management of the patients. Thus, this paper presents a mathematical model to study the dynamics and control of COVID-19-TB co-infection. The full model of the co-infection is split into two submodels, namely, the TB-only and the COVID-19-only models. The equilibria of the disease-free and endemic situations of the two sub-models are shown to be globally asymptotically stable when their control reproduction numbers $R_o^{TV}, R_o^{CV} < 1$ and $\tilde{R}_o^{TV}, \tilde{R}_o^{CV} > 1$, respectively. However, the disease-free equilibrium of the co-infection model was found to lose its global stability property when the reproduction number $R_o^F < 1$, therefore exhibiting a backward bifurcation. Uncertainty and sensitivity analysis of the associated reproduction number of the full model has been performed by using the Latin hypercube sampling/Pearson rank correlation coefficient (LHS/PRCC) method. The rate of transmission of COVID-19 and the proportions of individuals vaccinated with Bacillus Calmette-Guérin (BCG) and against COVID-19 were found to be highly significant in the spread and control of COVID-19-TB co-infection. Furthermore, the simulation results show that decreasing the COVID-19 transmission rate and increasing the proportion of people vaccinated with BCG and against COVID-19 can lower the number of cases of COVID-19-TB co-infection. Therefore, measures to reduce the transmission rate and the provision of adequate resources to increase the proportions of people vaccinated against TB and COVID-19 should be implemented to minimize the cases of co-infection.

Keywords: COVID-19-TB co-infection; COVID-19; TB; vaccination; equilibrium state

1. Introduction

COVID-19 began its widespread propagation in Wuhan, China in December 2019 and spread throughout the World, with devastating effects on the health and lives of people. Currently, there are 760 million confirmed cases of the COVID-19 in the world, and 6.9 million people have been reported to have died from the infection [1]. COVID-19 is a contagious disease caused by SARS-CoV-2. The disease is characterized by respiratory symptoms which are similar to the flu, a cold, or pneumonia, and it spreads primarily through the droplets from an infected person. It mainly attacks the lungs and respiratory organs [2].

Tuberculosis (TB) is a serious respiratory disease which has continued to impact the health of people negatively. The causative agent of TB is *Mycobacterium TB*, which attacks the lungs [3]. One of the main barriers to the fight against TB is the resistance of *Mycobacterium TB* to drugs. Globally, TB ranks thirteenth among diseases with a high mortality rate, and it is the second infectious killer disease after COVID-19. In 2021, about 10.6 million people contracted TB, and a total of 1.6 million deaths occurred as a result of TB worldwide [4].

Both COVID-19 and TB are infectious diseases and they attack the lungs. The two diseases have similar manifestations, such as fever, cough, and breathing problems. However, the latency period of COVID-19 is shorter than that of TB [4]. The experience of COVID-19 infection in people with TB is still limited, but it is expected that people with COVID-19-TB co-infection will experience worse treatment results, especially if TB treatment is interrupted [4].

Clinical studies have reported and discussed the possibility, interaction, and facilitation of dual infections. According to Yang and Lu [5], they opined that the intake of immunosuppressive drugs by people infected with the COVID-19 can temporarily alter immunological functionality, introducing vulnerability to active TB via a new infection or reinfection. Also, from the pathological point of view, the immunomodulation-related disorders caused by the pathogens of COVID-19 and TB lead to an unstable inflammatory response and progression and worsening of the two diseases [6]. According to [7], there is a huge reduction in T cell counts in patients with COVID-19, and Khayat et al. [8] stated that T cell depletion can cause the patient to develop active TB if the patient is living with latent TB. In a pilot study carried out by the Global Tuberculosis Network, the diagnosis of TB and COVID-19 was concurrently carried out in patients, and a clinical investigation of COVID-19 in patients led to the discovery of TB [9].

Opportunistic infections typically refer to infections that occur in people with weak immune systems, such as those with HIV/AIDS or those on immunosuppressants therapy. According to a previous study [10], COVID-19 can also be referred to as an opportunistic infection. These infections take advantage of the compromised immune system to cause illness. In the case of a co-infection of COVID-19 and TB, COVID-19 is considered to be an opportunistic infection; similarly, both diseases can independently cause illness in individuals with normal or compromised immune systems. However, having both infections simultaneously could potentially exacerbate symptoms and increase the severity of the disease, particularly in people with underlying health conditions or weak immune systems. The estimated efficacy of the Bacillus Calmette-Guérin (BCG) vaccine is about 50–60% in childhood TB prevention.

Recently, the modeling of the spread of contagious diseases has come to influence the theory and practice of disease control and management. Mathematical modeling now plays an important role in epidemiology-related policy decision-making for diseases in many countries [11]. Several studies have been carried out on TB and COVID-19 dynamics, with remarkable results. The authors of [12] proposed a model for the prevention and control of TB by using cases from US citizens. Also, Nkamba et al. [13] worked on the TB mathematical model to examine the influence of vaccination and the effective contact rate. In addition, Liu et al. [14] formulated a mathematical model to study China's transmission of TB. The authors used data from reported cases of TB in China from 1998 to 2017 to calibrate the model. In a study by Chong et al. [15], a model was used to investigate the effect of treatment on latent TB infection in the elderly population. Researchers including Perkins and España [16], Oke et al. [17], Zamir et al. [18], Masandawa et al. [19], Atede et al. [20] etc., have worked on the modelling of COVID-19. Also, Yang et al. [21] investigated the impact of vaccination in the COVID-19 transmission model, and the model was later extended to incorporate isolation as an intervention. The work of Kouidere et al. suggested that the awareness and quarantine of people infected with COVID-19 are the most effective means of reducing infection [22]. Furthermore, Ngonghala et al. [23] examined the impact of nonpharmaceutical measures on mitigating the burden of COVID-19. They concluded that early implementation, strict adherence, and high coverage of measures such as combinations of face mask use and social distancing in the public can reduce disease transmission.

Many models of co-infection of diseases have been formulated and studied [24–28]. The authors of [29] presented a mathematical analysis and numerical solutions of a model for the co-infection of TB-HIV. The authors of [30] studied the optimal control and cost-effectiveness of the human papillomavirus and syphilis co-infection model. The authors of [31] presented the COVID-19 and TB co-infection model by using the Atangana–Baleanu derivative in the fractional-order approach. In the same vein, the authors of [32] developed a fractional-order COVID-19 and hepatitis B virus co-infection model; they compared the approximate solutions of models of integer and fractional order. Another group of authors [33] developed the SARS-CoV-2 and TB

co-infection model to study its optimal control by using a case from Indonesia. Also, Gweryina et al. [34] worked on a model of TB co-infected with pneumonia. The authors of [35] presented a seven-compartment TB-COVID-19 co-infection model. Similarly, Mekonen et al. [36] studied and analyzed a mathematical model of TB and COVID-19 co-infection, and their analysis revealed that minimizing the contact rate and increasing treatments can reduce the cases of co-infection with COVID-19-TB. The authors of [37] studied a fractal-fractional model of TB and COVID-19 co-infection by using the Atangana-Baleanu fractal-fractional operator; additionally Lagrange polynomial interpolation was used to obtain the numerical scheme for the co-infection model. Also, Bandekar and Ghosh conducted optimal control and sensitivity analysis of the TB-COVID-19 co-infection model [38]. Their work emphasized that the treatment of other diseases should be implemented in times of a pandemic. Furthermore, Inayaturohmat et al. [39] examined the effects of treatment and isolation on a co-infection model of TB and COVID-19. Their results revealed that the impact of isolation is immediate, whereas the treatment takes a longer time for its effect to be felt.

In another study, Kifle and Obsu [40] applied optimal control in their COVID-19-TB co-infection model. They incorporated exogenous TB reinfection and COVID-19 vaccination into the model.

The authors of [41] developed a compartmental model to analyze the spread of HIV/AIDS-TB co-infection. They considered preventive measures and the treatment of infected individuals and assessed the impact of co-infection and single-infection treatment on the spreading dynamics of HIV/AIDS-TB co-infection and single infection. The study concluded that therapeutic controls were more effective for infected individuals, whereas preventive controls were more effective for noninfected individuals. In another study, Kotola et al. [42] formulated and analyzed a mathematical model for the transmission dynamics of HIV/AIDS and COVID-19 co-infection. Their model incorporated protection and treatment for infected groups. The results showed that applying combinations of all possible protective and treatment strategies was the most effective strategy to minimize the transmission of HIV/AIDS and COVID-19 co-infection in the community.

Similarly, Teklu [43] investigated the respective impacts of vaccination, other protective measures, home quarantine with treatment, and hospital quarantine with treatment strategies simultaneously by using a deterministic mathematical modeling approach. They found that, among all parameters, the transmission rate is the most sensitive to control, and that vaccination, other protective measures, home quarantine with treatment, and hospital quarantine with treatment greatly minimize COVID-19 transmission in the community.

In addition, the authors of [44] studied a compartmental model of co-infection of pneumonia and HIV/AIDS with optimal control strategies by using a system of ordinary differential equations. They investigated various optimal control strategies to predict the best strategy to minimize and possibly eradicate HIV/AIDS and pneumonia co-infection from the community.

However, none of the studies has incorporated a vaccination program for the two diseases, and this makes our current research differ from the existing works. Since TB and COVID-19 are infectious diseases with similar clinical manifestations, they mainly attack the lungs. Clinical studies have revealed that the immunosuppressive drugs taken by COVID-19 patients can affect the immunological functions in the body, which can make patients vulnerable to active TB via a new infection or reinfection; also, the co-infection of the two diseases portends a clinical complexity in the management of the patients. This has motivated us to present a mathematical model that studied the dynamics and control of COVID-19-TB co-infection.

We also aimed to identify which parameters actually trigger the burden of COVID-19-TB co-infection, as well as the parameters that must be targeted in order to reduce the incidence of either disease in the population as this will allow us to appropriately advise policymakers, health workers, and government agencies.

It is important to note that this study is limited to the use of classical ordinary differential equations in the modeling process.

The other part of this work is fragmented into sections as follows: Section 2 presents the formulation of the model, the analysis of the model is given in Section 3, the discussion of the results follows in Section 4, and the conclusion is in Section 5.

2. Mathematical formulation and the assumptions of the model

The total human population (N) at time (t) is separated into the following classes: the susceptible ($S(t)$) class, the latent TB ($L_T(t)$) class, the TB infectious class ($I_T(t)$), the latent COVID-19 ($L_C(t)$) class, the COVID-19 infectious class ($I_C(t)$), the latent COVID-19-TB co-infected class ($L_{TC}(t)$), the infectious COVID-19-TB co-infected class ($I_{TC}(t)$), the treatment ($T(t)$) class, the class of individuals who are vaccinated ($V(t)$), and the recovered class ($R(t)$). It is assumed that the susceptible class ($S(t)$) is increased by the recruitment of people (at the rate Λ). This class diminishes as a result of infections following contact with TB-infectious individuals, COVID-19-infectious individuals, infectious COVID-19-TB co-infected individuals at the rates λ_C and λ_T, given by

$$\lambda_T = \frac{\beta_1(I_T + mI_{TC})}{N} \quad \text{and} \quad \lambda_C = \frac{\beta_2(I_C + nI_{TC})}{N}, \tag{2.1}$$

where β_1 and β_2 are the transmission rates of TB and the COVID-19 infections, respectively. Also, m and n are the modification parameters accounting for reduced infectivity of the I_{TC} class relative to the I_T and I_C classes, respectively. The class further reduces due to the vaccination of proportions a and b of the newly recruited individuals against TB and COVID-19 infection respectively. It is also assumed that all humans die naturally (at the rate μ), which causes every compartment to reduce. Therefore,

$$\frac{dS}{dt} = (1 - (a + b))\Lambda - \lambda_T S - \lambda_C S - \mu S. \tag{2.2}$$

The class L_T of people with latent TB is assumed to be populated by the newly infected TB individuals who have acquired TB (at the rate λ_T). The size of the class diminishes due to transfer (at the rates α and η) to the I_T class and L_{TC} class, respectively. Thus,

$$\frac{dL_T}{dt} = \lambda_T S - (\mu + \alpha + \eta\lambda_C)L_T. \tag{2.3}$$

The TB infectious class (I_T) is assumed to be composed of those who have transitioned from the latent class (at the rate α); additionally, the size of the class shrinks due to progression (at the rates γ and θ). Thus,

$$\frac{dI_T}{dt} = \alpha L_T - (\mu + \delta_T + \gamma + \theta)I_T. \tag{2.4}$$

The latent COVID-19 class (L_C) comprises those who just contracted COVID-19 (at the rate λ_C). This population is decreased by transition to the I_C and L_{TC} classes (at the rates ψ and ε, respectively). Also, the population of individuals with latent COVID-19 declines (at the rate χ) as they recover naturally without treatment. Hence,

$$\frac{dL_C}{dt} = \lambda_C S - (\mu + \chi + \varepsilon\lambda_T + \psi)L_C. \tag{2.5}$$

The class I_C, of infectious COVID-19 individuals is occupied by those who have transitioned into the class from the L_C compartment (at the rate ψ). The reductions in the I_C population are caused by mortality (at the rate δ_C) and transition to the I_{TC} and T classes (at the rates υ and φ, respectively). Therefore,

$$\frac{dI_C}{dt} = \psi L_C - (\mu + \delta_C + \upsilon + \varphi)I_C. \tag{2.6}$$

The L_{TC} population of the latent COVID-19-TB co-infected individuals is assumed to be generated by the latent COVID-19 individuals who contracted TB and latent-TB-infected individuals who contracted COVID-19 as well. The transition to the class I_{TC} (at the rate ρ) lowers this population. Hence,

$$\frac{dL_{TC}}{dt} = \eta\lambda_C L_T + \varepsilon\lambda_T L_C - (\mu + \rho)L_{TC}. \tag{2.7}$$

The I_{TC} class is increased by the contributions of the L_{TC}, I_T, and I_C classes (at the rates γ, θ, and υ, respectively), indicating infectious COVID-19-TB co-infected. The treatment and death due to the co-infection (at the rates τ and δ_{TC}, respectively) cause the population to reduce. Thus,

$$\frac{dI_{TC}}{dt} = \rho L_{TC} + \theta I_T + \upsilon I_C - (\mu + \delta_{TC} + \tau)I_{TC}. \tag{2.8}$$

The treatment class is filled with those who are receiving treatment in the I_T, I_C, and I_{TC} classes (at the rates γ, φ, and τ, respectively). The class is decreased by recovery at the rate ϕ. Then,

$$\frac{dT}{dt} = \gamma I_T + \varphi I_C + \tau I_{TC} - (\phi + \mu)T. \tag{2.9}$$

It is assumed that the vaccinated class V has the proportions a and b of those that are recruited who have been vaccinated against TB and COVID-19. Then,

$$\frac{dV}{dt} = a\Lambda + b\Lambda - \mu V. \tag{2.10}$$

Last, the recovered compartment comprises those recovered from treatment at the rate ϕ and those who recover at the rate χ from latent COVID-19 naturally without treatment. Thus,

$$\frac{dR}{dt} = \phi T + \chi L_C - \mu R. \tag{2.11}$$

The schematic diagram illustrating the dynamics in the models is given in Figure 1. Also, all of the parameters and variables used in the model are defined in Tables 1 and 2.

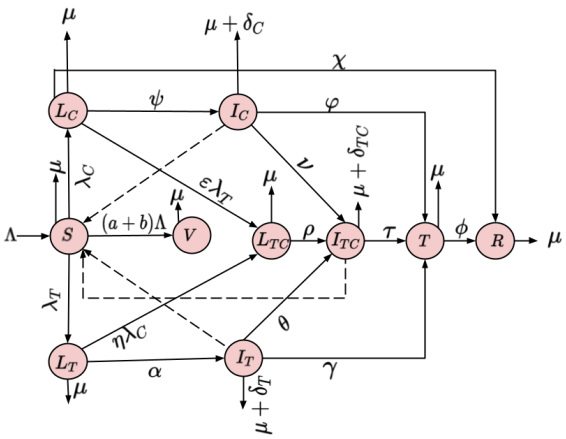

Figure 1. Schematic diagram of the dynamics of the COVID-19-TB co-infection model.

Table 1. The description of variables of the COVID-19-TB co-infected model (2.12).

Parameter	Description
$S(t)$	Susceptible class
$L_T(t)$	Latent TB class
$I_T(t)$	TB-infectious class
$L_C(t)$	Latent COVID-19 class
$I_C(t)$	COVID-19 infectious class
$L_{TC}(t)$	Latent COVID-19-TB co-infected class
$I_{TC}(t)$	Infectious COVID-19-TB co-infected class
$T(t)$	Class of individuals under treatment
$V(t)$	Class of individuals who are vaccinated
$R(t)$	Recovered class

Table 2. Definition and value of each parameter of the model (2.12).

Parameter	Definition	Value	Reference
Λ	Recruitment rate for the population	20	Assumed
β_1	Transmission rate of TB infection	0.0234	[45]
β_2	Transmission rate of COVID-19 infection	0.49	[46]
m, n	Modification parameters accounting for reduced infectivity of TB and COVID-19	0.1,0.1	Assumed
μ	Natural death rate for humans	0.0000423	[38]
α	Progression of latent TB individuals to TB infectious class	0.000137	[45]
η	Rate at which latent TB individuals become latently infected with COVID-19	0.2	Assumed
γ	Treatment rate for TB-infectious individuals	0.1005	[39]
χ	Recovery rate for latent COVID-19 individuals	0.00001	Assumed
ψ	Progression of latent COVID-19 individuals to infectious COVID-19 class	0.087	[47]
ε	Rate at which latent COVID-19 individuals become latently infected with TB	0.2	Assumed
υ	Rate at which COVID-19-infectious humans become actively infected with TB	0.039	Assumed
θ	Rate at which TB-infectious human becomes actively infected with COVID-19	0.25	[48]
φ	Treatment rate for COVID-19-infectious individuals	0.0264	[49]
a	Proportion of individuals vaccinated with BCG	0.1	Assumed
b	Proportion of individuals vaccinated against COVID-19	0.1	Assumed
δ_T	Induced death rate for TB	0.001	[45]
δ_C	Induced death rate for COVID-19	0.20704	[17]
δ_{TC}	Induced death rate for co-infection	0.0525	[39]
ρ	Progression of individuals from L_{TC} to I_{TC}	0.05	Assumed
τ	Treatment rate for co-infected individuals	0.0055	Assumed
ϕ	Recovery rate of treated individuals	0.018	Assumed
λ_T, λ_C	Forces of infection for TB and COVID-19	—	—

Summarily, combining all of the assumptions together, we have the following system of equations:

$$\begin{cases} \dfrac{dS}{dt} = (1-(a+b))\Lambda - \lambda_T S - \lambda_C S - \mu S, \\ \dfrac{dL_T}{dt} = \lambda_T S - (\mu+\alpha+\eta\lambda_C)L_T, \\ \dfrac{dI_T}{dt} = \alpha L_T - (\mu+\delta_T+\gamma+\theta)I_T, \\ \dfrac{dL_C}{dt} = \lambda_C S - (\mu+\chi+\varepsilon\lambda_T+\psi)L_C, \\ \dfrac{dI_C}{dt} = \psi L_C - (\mu+\delta_C+\upsilon+\varphi)I_C, \\ \dfrac{dL_{TC}}{dt} = \eta\lambda_C L_T + \varepsilon\lambda_T L_C - (\mu+\rho)L_{TC}, \\ \dfrac{dI_{TC}}{dt} = \rho L_{TC} + \theta I_T + \upsilon I_C - (\mu+\delta_{TC}+\tau)I_{TC}, \\ \dfrac{dT}{dt} = \gamma I_T + \varphi I_C + \tau I_{TC} - (\phi+\mu)T, \\ \dfrac{dV}{dt} = a\Lambda + b\Lambda - \mu V, \\ \dfrac{dR}{dt} = \phi T + \chi L_C - \mu R, \end{cases} \tag{2.12}$$

where

$$\lambda_T = \frac{\beta_1(I_T + mI_{TC})}{N}, \quad \lambda_C = \frac{\beta_2(I_C + nI_{TC})}{N}.$$

2.1. Positivity of the solutions

Since the model (2.12) tracks the populations of humans, the solutions to the model (2.12) have to be positive. Hence, the following theorem is proved to ensure that the solutions are all positive.

Theorem 2.1. *All solutions*

$$S(t), L_T(t), I_T(t), L_C(t), I_C(t), L_{TC}(t), I_{TC}(t), T(t), V(t), R(t)$$

having positive starting values continue to be positive at all times.

Proof. Let $t_1 = sup\{t > 0 : S(t) > 0, L_T(t) > 0, I_T(t) > 0, L_C(t) > 0, I_C(t) > 0, L_{TC}(t) > 0, I_{TC}(t) > 0, T(t) > 0, V(t) > 0, R(t) > 0\} > 0$.

So, from the equation for the first compartment of the model (2.12), we have

$$\frac{dS}{dt} = (1-(a+b))\Lambda - \lambda_T S - \lambda_C S - \mu S. \tag{2.13}$$

Then,

$$\frac{dS}{dt} \geq (-\lambda_T - \lambda_C - \mu)S, \tag{2.14}$$

$$\int_0^{t_1} \frac{dS}{S} \geq \int_0^{t_1} -(\lambda_T + \lambda_C + \mu)dt, \tag{2.15}$$

$$S(t) \geq S(0)\exp\left(-\mu t_1 - \int_0^{t_1}(\lambda_T(\chi) + \lambda_C(\chi))d\chi\right) \geq 0.$$

$$\therefore S(t_1) \geq 0. \tag{2.16}$$

By applying the same approach, all other variables of the model (2.12) can be shown to stay positive for all time $t > 0$; therefore, this ends the proof. □

2.2. Invariant region of the model

Lemma 2.1. *Consider*

$$D = \left\{(S, L_T, I_T, L_C, I_C, L_{TC}, I_{TC}, T, V, R) \in R_+^{10} : N \leq \frac{\Lambda}{\mu}\right\}.$$

Then, the closed set D is positively-invariant and attracting for the model (2.12)*.*

Proof. The summation of the rates of change of all classes in (2.12) gives

$$\frac{dN}{dt} = \Lambda - \mu N - \delta_T I_T - \delta_C I_C - \delta_{TC} I_{TC}.$$

So,

$$\frac{dN}{dt} \leq \Lambda - \mu N.$$

Then

$$N(t) \leq N(0)e^{-\mu t} + \frac{\Lambda}{\mu}(1 - e^{-\mu t}).$$

If

$$N(0) \leq \frac{\Lambda}{\mu},$$

then

$$N(t) \leq \frac{\Lambda}{\mu}.$$

Hence, all solutions possessing initial values in D stay in D for $t > 0$. This signifies that D is positively-invariant, and that, in region D, the model is deemed to be epidemiologically meaningful and mathematically well-posed. □

3. Mathematical analysis of the models

The full co-infection model is split into 2 sub-models namely, the TB-only model and the COVID-19-only model. We will first explore the dynamics of the 2 sub-models separately (i.e., the TB-only model and the COVID-19-only model) before proceeding to the co-infection model.

3.1. TB-only model

The TB-only model is obtained from the co-infection model (2.12) by setting $b = \theta = 0$ and $L_C = I_C = L_{TC} = I_{TC} = 0$; thus we have the TB-only model as follows:

$$\begin{cases} \dfrac{dS}{dt} = (1-a)\Lambda - \lambda_T S - \mu S, \\ \dfrac{dL_T}{dt} = \lambda_T S - (\mu+\alpha)L_T, \\ \dfrac{dI_T}{dt} = \alpha L_T - (\mu+\delta_T+\gamma)I_T, \\ \dfrac{dT}{dt} = \gamma I_T - (\phi+\mu)T, \\ \dfrac{dV}{dt} = a\Lambda - \mu V, \\ \dfrac{dR}{dt} = \phi T - \mu R, \end{cases} \tag{3.1}$$

where

$$\lambda_T = \frac{\beta_1 I_T}{N}, \tag{3.2}$$

$$N = S + L_T + I_T + T + V + R. \tag{3.3}$$

Consider the feasible region

$$D_T = \left\{(S, L_T, I_T, T, V, R) \in R_+^6 : N \le \frac{\Lambda}{\mu}\right\}.$$

It can be shown that all solutions in D_T stay in D_T for all values of $t > 0$. Hence, D_T is positively-invariant. Now, we can proceed to explore the model's dynamics in D_T.

3.1.1. Disease-free equilibrium and reproduction number of TB-only model

When TB infection does not exist, the disease-free equilibrium is obtained, and it is given by

$$\begin{aligned} E_T^o &= (S^o, L_T^o, I_T^o, T^o, V^o, R^o) \\ &= \left(\frac{(1-a)\Lambda}{\mu}, 0, 0, 0, \frac{a\Lambda}{\mu}, 0\right). \end{aligned} \tag{3.4}$$

By adopting the next-generation matrix method of [50] to find the reproduction number, we can respectively define the matrices F and V as follows:

$$F = \begin{pmatrix} \lambda_T S \\ 0 \\ 0 \end{pmatrix} \text{ and } V = \begin{pmatrix} (\mu+\alpha)L_T \\ -\alpha L_T + (\mu+\delta_T+\gamma)I_T \\ -\gamma I_T + (\phi+\mu)T \end{pmatrix}. \tag{3.5}$$

Differentiating F and V in (3.5) with respect to $L_T, I_T,$ and T at the disease-free equilibrium E_T^o, leads to

$$F = \begin{bmatrix} 0 & \beta_1(1-a) & 0 \\ 0 & 0 & 0 \\ 0 & 0 & 0 \end{bmatrix} \tag{3.6}$$

and

$$V = \begin{bmatrix} G_1 & 0 & 0 \\ -\alpha & G_2 & 0 \\ 0 & -\gamma & G_3 \end{bmatrix}, \tag{3.7}$$

where

$$G_1 = \mu + \alpha, \quad G_2 = \mu + \delta_T + \gamma, \quad G_3 = \phi + \mu. \tag{3.8}$$

Then, the control reproduction number in the presence of the vaccine, denoted by R_o^{TV}, is given by

$$R_o^{TV} = \rho(FV^{-}1) = \frac{\beta_1\alpha(1-a)}{G_1 G_2}. \tag{3.9}$$

The ρ parameter in (3.9) is the spectral radius of the dominant eigenvalue of the matrix FV^{-1}. When there is no vaccination, the basic reproduction number is represented by R_o^T, which is given by

$$R_o^T = \frac{\beta_1\alpha}{G_1 G_2}. \tag{3.10}$$

Then, from (3.9) and (3.10), we have that

$$R_o^{TV} = (1-a)R_o^T. \tag{3.11}$$

If we denote the critical vaccination proportion to be a_c, then, the critical number of individuals that must be vaccinated to guarantee the elimination of the disease is given by

$$a_c = 1 - \frac{1}{R_o^T}, \tag{3.12}$$

provided that $R_o^{TV} \le 1$ whenever $a \ge a_c$.

The epidemiological quantity R_o^{TV} is the control reproduction number, which is the average number of secondary TB infections that stem from one primary infection source when introduced into the population of susceptible individuals where a proportion a has been vaccinated. On the other hand, the quantity R_o^T is the basic reproduction number of the TB-only model. This is the average number of secondary TB infections that stemmed from a single infectious person in a group of susceptible individuals [50]. Therefore, employing Theorem 2 of [51], we arrive at the following result:

Lemma 3.1. *If $R_o^{TV} < 1$, then the disease-free equilibrium of TB-model* (3.1) *is locally asymptotically stable.*

The meaning of Lemma 3.1 is that the eradication of TB is possible if the starting values of the sub-classes of the model are in the basin of attraction of E_T^o. Therefore, an introduction of a small group of TB-infectious people into the population will not produce an outbreak of TB; therefore, it vanishes.

3.1.2. Endemic equilibrium of TB-only model

The endemic equilibrium of the TB-only model represented by

$$E_T^e = (S^*, L_T^*, I_T^*, T^*, V^*, R^*)$$

is obtained as follows:

$$\begin{cases} S^* = \dfrac{[(1-a)[\alpha\gamma G_3 + \mu G_3(\alpha + G_2)] + aG_1G_2G_3]\,\Lambda(1-a)}{[(1-a)[\alpha\gamma G_3 + \mu G_3(\alpha + G_2)] + G_1G_2G_3G_4]\mu}, \\ L_T^* = \dfrac{\Lambda G_2G_3(R_o^{TV} - 1)(1-a)}{[(1-a)[\alpha\gamma G_3 + \mu G_3(\alpha + G_2)] + G_1G_2G_3G_4]}, \\ I_T^* = \dfrac{\alpha\Lambda G_3(R_o^{TV} - 1)(1-a)}{[(1-a)[\alpha\gamma G_3 + \mu G_3(\alpha + G_2)] + G_1G_2G_3G_4]}, \\ T^* = \dfrac{\alpha\gamma\Lambda(R_o^{TV} - 1)(1-a)}{[(1-a)[\alpha\gamma G_3 + \mu G_3(\alpha + G_2)] + G_1G_2G_3G_4]}, \\ V^* = \dfrac{a\Lambda}{\mu}, \\ R^* = \dfrac{\phi\alpha\gamma\Lambda(R_o^{TV} - 1)(1-a)}{[(1-a)[\alpha\gamma G_3 + \mu G_3(\alpha + G_2)] + G_1G_2G_3G_4]}, \end{cases} \tag{3.13}$$

where G_1, G_2, and G_3 have been defined in (3.8); similarly,

$$G_4 = R_o^{TV} - 1 + a.$$

From (3.13), it is clear that E_T^e has a unique positive endemic equilibrium when $R_o^{TV} > 1$.

3.1.3. Global stability of disease-free equilibrium of TB-only model

The global asymptotic stability of the disease-free equilibrium of the TB-only model is investigated here for $R_o^{TV} < 1$, to determine whether the disappearance of TB is independent of the starting values of the sub-classes of the TB-only model.

Theorem 3.1. *The disease-free equilibrium* (3.4) *of the TB-only model* (3.1) *is globally asymptotically stable when $R_o^{TV} < 1$, but not when $R_o^{TV} > 1$.*

Proof. We apply linear Lyapunov function, which is given by

$$Z = \alpha L_T + G_1 I_T + \left(\frac{G_1G_2N - \alpha\beta_1 S}{N\gamma}\right) T. \tag{3.14}$$

The time derivative of (3.14) is given by

$$Z' = \alpha L_T' + G_1 I_T' + \left(\frac{G_1G_2N - \alpha\beta_1 S}{N\gamma}\right) T'. \tag{3.15}$$

Then, by substitution and simplification, we have

$$Z' = \frac{\alpha\beta_1 G_3 S T}{N\gamma} - \frac{G_1G_2G_3T}{\gamma},$$
$$Z' = \left(\frac{G_1G_2G_3T}{\gamma}\right)[R_o^{TV} - 1].$$

Therefore, $Z' < 0$ if $R_o^{TV} < 1$ and $Z' = 0$ if $T = 0$. Thus, Z is a Lyapunov function in D_T. Also, the largest invariant set in

$$(S, L_T, I_T, T, V, R) \in D_T : Z' = 0$$

is the singleton E_T^o. According to LaSalle's invariance principle [52], every solution that possesses initial values in D_T tends to E_T^o as t becomes large. □

Theorem 3.1, epidemiologically, means that TB can be curtailed regardless of the starting sizes of the sub-classes of the model (3.1) when $R_o^{TV} < 1$.

3.1.4. Global stability of endemic equilibrium of the TB-only model

Consider the model (3.1) with $\delta_T = 0$. Let

$$\tilde{\beta_1} = \frac{\beta_1\mu}{\Lambda}$$

and the endemic equilibrium be denoted by

$$E_T^{e*} = (S^{**}, L_T^{**}, I_T^{**}, T^{**}, V^{**}, R^{**}).$$

If the associated reproduction number of the model is given by

$$\tilde{R}_o^{TV} = R_{o|_{\delta_T=0}}^{TV} > 1.$$

Then, we prove the global stability of E_T^{e*}.

Theorem 3.2. *For $D_T \backslash D^*$, the endemic equilibrium of the model* (3.1) *with $\delta_T = 0$ is globally asymptotically stable if $\tilde{R}_o^{TV} > 1$, where*

$$D^* = \{(S, L_T, I_T, T, V, R) \in D_T : L_T = I_T = T = R = 0\}.$$

Proof. We apply the Lyapunov function in (3.16) to prove Theorem 3.2

$$\begin{aligned} Q = {} & S - S^{**} - S^{**} \ln \frac{S}{S^{**}} + L_T - L_T^{**} - L_T^{**} \ln \frac{L_T}{L_T^{**}} \\ & + \frac{G_1}{\alpha} \left[I_T - I_T^{**} - I_T^{*} \ln \frac{I_T}{IT^{**}} \right] \\ & + \frac{G_1 G_2 - \tilde{\beta}_1 S^{**} \alpha}{\alpha \gamma} \left[T - T^{**} - T^{**} \ln \frac{T}{T^{**}} \right]. \end{aligned} \tag{3.16}$$

By differentiation, (3.16) becomes

$$\begin{aligned} Q' = {} & \left(1 - \frac{S^{**}}{S}\right) S' + \left(1 - \frac{L_T^{*}}{L_T}\right) L_T' + \frac{G_1}{\alpha} \left[1 - \frac{I_T^{**}}{I_T}\right] I_T' \\ & + \frac{G_1 G_2 - \tilde{\beta}_1 S^{**} \alpha}{\alpha \gamma} \left[1 - \frac{T^{**}}{T}\right] T', \end{aligned} \tag{3.17}$$

$$\begin{aligned} Q' = {} & 3\tilde{\beta}_1 I_T^{**} S^{**} - 2\mu S^{**} - \mu S - \frac{\tilde{\beta}_1 I_T^{**} S^{*2}}{S} - \frac{\mu S^{**2}}{S} \\ & - \frac{\tilde{\beta}_1 I_T S L_T^{**}}{L_T} - \frac{\tilde{\beta}_1 I_T^{**} S^{**} L_T I_T^{**}}{I_T L_T^{**}}, \end{aligned} \tag{3.18}$$

$$\begin{aligned} Q' = {} & \tilde{\beta}_1 I_T^{**} S^{**} \left(3 - \frac{S^{**}}{S} - \frac{I_T S L_T^{**}}{I_T^{**} S^{**} L_T} - \frac{I_T^{**} L_T}{L_T^{**} I_T}\right) \\ & + \mu S^{**} \left(2 - \frac{S}{S^{**}} - \frac{S^{**}}{S}\right). \end{aligned} \tag{3.19}$$

With the arithmetic mean surpassing the geometric mean, we have the following inequalities:

$$3 - \frac{S^{**}}{S} - \frac{I_T S L_T^{**}}{I_T^{**} S^{**} L_T} - \frac{I_T^{**} L_T}{L_T^{**} I_T} \leq 0$$

and

$$2 - \frac{S}{S^{**}} - \frac{S^{**}}{S} \leq 0.$$

Hence, $Q' \leq 0$ for $\tilde{R}_o^{TV} > 1$. Therefore, Q is a Lyapunov function in D_T, and, from LaSalle's invariance principle [52], every solution possessing starting values in $D_T \backslash D^*$ tends to E_T^{e*} as the time moves closer to infinity for $\tilde{R}_o^{TV} > 1$. □

The biological interpretation of Theorem 3.2 is that TB will continue to exist in the community regardless of the initial population levels whenever $\tilde{R}_o^{TV} > 1$.

3.2. COVID-19-only model

The COVID-19-only model can be obtained from the co-infection model (2.12) when

$$a = \upsilon = 0$$

and

$$L_T = I_T = L_{TC} = I_{TC} = 0.$$

We have the COVID-19-only model as follows:

$$\begin{cases} \dfrac{dS}{dt} = (1-b)\Lambda - \lambda_C S - \mu S, \\ \dfrac{dL_C}{dt} = \lambda_C S - (\mu + \chi + \psi) L_C, \\ \dfrac{dI_C}{dt} = \psi L_C - (\mu + \delta_C + \varphi) I_C, \\ \dfrac{dT}{dt} = \varphi I_C - (\phi + \mu) T, \\ \dfrac{dV}{dt} = b\Lambda - \mu V, \\ \dfrac{dR}{dt} = \phi T + \chi L_C - \mu R, \end{cases} \tag{3.20}$$

where

$$\lambda_C = \frac{\beta_2 I_C}{N}, \tag{3.21}$$

$$N = S + L_C + I_C + T + V + R. \tag{3.22}$$

Regarding model (3.20), it can be shown that the region given by

$$D_C = \left\{ (S, L_C, I_C, T, V, R) \in R_+^6 : N \leq \frac{\Lambda}{\mu} \right\}$$

is positively-invariant and attracting. Then, the COVID-19-only model (3.20) will be considered in the region D_C.

3.2.1. Disease-free equilibrium and reproduction number of COVID-19-only model

In a case in which there is no COVID-19, we have a disease-free situation, and its equilibrium is given by

$$\begin{aligned} E_C^o &= (S^o, L_C^o, I_C^o, T^o, V^o, R^o) \\ &= \left(\frac{(1-b)\Lambda}{\mu}, 0, 0, 0, \frac{b\Lambda}{\mu}, 0 \right). \end{aligned} \tag{3.23}$$

The control reproduction number of COVID-19 is obtained by employing the next-generation matrix method as in [50]. Let F and V be defined as follows:

$$F = \begin{bmatrix} 0 & \beta_1(1-b) & 0 \\ 0 & 0 & 0 \\ 0 & 0 & 0 \end{bmatrix} \tag{3.24}$$

and

$$V = \begin{bmatrix} H_1 & 0 & 0 \\ -\psi & H_2 & 0 \\ 0 & -\varphi & H_3 \end{bmatrix}. \tag{3.25}$$

Then, the control reproduction number is given by

$$R_o^{CV} = \rho(FV^{-1}1) = \frac{\beta_2\psi(1-b)}{H_1H_2}, \tag{3.26}$$

where

$$H_1 = \mu + \chi + \psi, \quad H_2 = \mu + \delta_C + \varphi, \tag{3.27}$$

and ρ is the spectral radius of the dominant eigenvalue of the matrix FV^{-1}. In the absence of a vaccine, the basic reproduction number is obtained, which is represented by R_o^C. Then,

$$R_o^C = \frac{\beta_2\psi}{H_1H_2}. \tag{3.28}$$

We can re-write (3.26) as follows:

$$R_o^{CV} = (1-b)R_o^C. \tag{3.29}$$

Thus, the critical number of individuals who need to be vaccinated to eliminate the disease is given by

$$b_c = 1 - \frac{1}{R_o^C}, \tag{3.30}$$

such that $R_o^{CV} \leq 1$ whenever $b \geq b_c$. Then, by adopting Theorem 2 of [51], we obtain the following result:

Lemma 3.2. *If $R_o^{CV} < 1$, then the disease-free equilibrium of the COVID-19-only model* (3.20) *is locally asymptotically stable.*

Lemma 3.2 basically states that the eradication of the COVID-19 is possible if the starting values of the different populations that make up the model are in the basin of attraction of E_C^o. Hence, an introduction of a few numbers of infected people into the population will not lead to an outbreak of COVID-19; then, the disease vanishes.

3.2.2. Endemic equilibrium of COVID-19-only model

Let the endemic equilibrium of the COVID-19-only model be represented by E_C^e. We obtain the following for E_C^e:

$$E_C^e = (S^*, L_C^*, I_C^*, T^*, V^*, R^*).$$

where

$$\begin{cases} S^* = \dfrac{[(1-b)[\psi(\varphi+\mu) + H_2(\mu+\chi)] + bH_1H_2]\,H_5}{[(1-b)[H_2(\chi+\mu) + \psi(\varphi+\mu)] + H_1H_2H_4]\mu}, \\ L_C^* = \dfrac{H_5H_2(R_o^{CV}-1)}{[(1-b)[H_2(\chi+\mu) + \psi(\varphi+\mu)] + H_1H_2H_4]}, \\ I_C^* = \dfrac{H_5\psi(R_o^{CV}-1)}{[(1-b)[H_2(\chi+\mu) + \psi(\varphi+\mu)] + H_1H_2H_4]}, \\ T^* = \dfrac{\varphi\psi H_5(R_o^{CV}-1)}{[(1-b)[H_2(\chi+\mu) + \psi(\varphi+\mu)] + H_1H_2H_4]H_3}, \\ V^* = \dfrac{b\Lambda}{\mu}, \\ R^* = \dfrac{H_5(R_o^{CV}-1)[\chi H_2H_3 + \varphi\phi\psi]}{[(1-b)[H_2(\chi+\mu) + \psi(\varphi+\mu)] + H_1H_2H_4]H_3}, \end{cases} \tag{3.31}$$

where

$$H_5 = \Lambda(1-b), \quad H_4 = R_o^{CV} - 1 + b, \quad H_3 = \phi + \mu,$$

and H_1 and H_2 have been defined in (3.27).

Evidently, from (3.31), we have a unique positive endemic equilibrium when $R_o^{CV} > 1$.

3.2.3. Global stability of disease-free equilibrium of COVID-19-only model

We shall investigate whether the elimination of COVID-19 relies on the starting values of the sub-classes through the exploration of the global asymptotic stability of the disease-free equilibrium of the COVID-19-only model.

Theorem 3.3. *The disease-free equilibrium* (3.23) *of the COVID-19-only model* (3.20) *is globally asymptotically stable when $R_o^{CV} < 1$, but not when $R_o^{CV} > 1$.*

Proof. We adopt the linear Lyapunov function defined by

$$J = \psi L_C + H_1 I_C + \left(\frac{H_1H_2N - \psi\beta_2 S}{N\varphi}\right)T. \tag{3.32}$$

Taking the derivative of (3.32) leads to

$$\frac{dJ}{dt} = \psi\frac{dL_C}{dt} + H_1\frac{dI_C}{dt} + \left(\frac{H_1H_2N - \psi\beta_2 S}{N\varphi}\right)\frac{dT}{dt}. \tag{3.33}$$

Then, by substitution and simplification, we have

$$\frac{dJ}{dt} = \frac{\psi\beta_2H_3ST}{N\varphi} - \frac{H_1H_2H_3T}{\varphi},$$
$$\frac{dJ}{dt} = \left(\frac{H_1H_2H_3T}{\varphi}\right)[R_o^{CV} - 1].$$

Therefore,

$$\frac{dJ}{dt} < 0$$

if $R_o^{CV} < 1$ and

$$\frac{dJ}{dt} = 0$$

if $T = 0$. Thus, J is a Lyapunov function in D_C. Also, the largest invariant set in

$$(S, L_C, I_C, T, V, R) \in D_C : \frac{dJ}{dt} = 0$$

is the singleton E_C^o. According to LaSalle's invariance principle [52], all solutions having initial values in D_C move toward E_C^o as t becomes large. □

Theorem 3.3 can be interpreted epidemiologically to mean that COVID-19 can be curbed regardless of the starting sizes of the sub-classes of the model (3.1) when $R_o^{CV} < 1$.

3.2.4. Global stability of endemic equilibrium of the COVID-19-only model

Consider the model (3.20) with $\delta_C = 0$. Let the associated transmission rate

$$\tilde{\beta_2} = \frac{\beta_2 \mu}{\Lambda},$$

and the endemic equilibrium be denoted by

$$E_C^{e*} = (S^{**}, L_C^{**}, I_C^{**}, T^{**}, V^{**}, R^{**}).$$

Let the associated reproduction number of the model be given by

$$\tilde{R}_o^{CV} = R_{o_{|\delta_C=0}}^{CV} > 1.$$

Then, we explore the global asymptotic behavior of E_C^{e*}.

Theorem 3.4. *For $D_C \backslash D^{**}$, the endemic equilibrium of the model* (3.20) *with $\delta_C = 0$ is globally asymptotically stable if $\tilde{R}_o^{CV} > 1$, where*

$$D^{**} = \{(S, L_C, I_C, T, V, R) \in D_C : L_C = I_C = T = R = 0\}.$$

Proof. We consider the Lyapunov function for the proof. We define the Lyapunov function as follows:

$$\begin{aligned} X = {} & S - S^{**} - S^{**} \ln \frac{S}{S^{**}} + L_C - L_C^{**} - L_C^{**} \ln \frac{L_C}{L_C^{**}} \\ & + \frac{H_1}{\psi} \left[I_C - I_C^{**} - I_C^{**} \ln \frac{I_C}{IC^{**}} \right] \\ & + \frac{H_1 H_2 - \tilde{\beta_2} S^{**} \psi}{\varphi \psi} \left[T - T^{**} - T^{**} \ln \frac{T}{T^{**}} \right]. \end{aligned} \tag{3.34}$$

By differentiation, (3.34) becomes

$$\begin{aligned} X' = {} & \left(1 - \frac{S^{**}}{S}\right) S' + \left(1 - \frac{L_C^{**}}{L_C}\right) L_C' + \frac{H_1}{\psi} \left[1 - \frac{I_C^{**}}{I_C}\right] I_C' \\ & + \frac{H_1 H_2 - \tilde{\beta_2} S^{**} \psi}{\varphi \psi} \left[1 - \frac{T^{**}}{T}\right] T', \end{aligned} \tag{3.35}$$

$$\begin{aligned} X' = {} & 3\tilde{\beta_2} I_C^{**} S^{**} - 2\mu S^{**} - \mu S - \frac{-\tilde{\beta_2} I_C^{**} S^{**2}}{S} - \frac{\mu S^{**2}}{S} \\ & - \frac{-\tilde{\beta_2} I_C S L_C^{**}}{L_C} - \frac{-\tilde{\beta_2} I_C^{**} S^{**} L_C I_C^{**}}{I_C L_C^{**}}, \end{aligned} \tag{3.36}$$

$$\begin{aligned} X' = {} & \tilde{\beta_2} I_C^{**} S^{**} \left(3 - \frac{S^{**}}{S} - \frac{I_C S L_C^{**}}{I_C^{**} S^{**} L_C} - \frac{I_C^{**} L_C}{L_C^{**} I_C}\right) \\ & + \mu S^{**} \left(2 - \frac{S}{S^{**}} - \frac{S^{**}}{S}\right). \end{aligned} \tag{3.37}$$

Given that the arithmetic mean surpassing the geometric mean, the following inequalities hold:

$$3 - \frac{S^{**}}{S} - \frac{I_C S L_C^{**}}{I_C^{**} S^{**} L_C} - \frac{I_C^{**} L_C}{L_C^{**} I_C} \leq 0, \quad 2 - \frac{S}{S^{**}} - \frac{S^{**}}{S} \leq 0.$$

Thus, $X' \leq 0$ for $\tilde{R}_o^{CV} > 1$. Then, X is a Lyapunov function in D_C, and from LaSalle's invariance principle [52], every solution with starting values in $D_C \backslash D^{**}$ tends to E_C^{e*} as the time moves closer to infinity for $\tilde{R}_o^{CV} > 1$. □

The biological interpretation of Theorem 3.4 is that COVID-19 will continue to exist in the population regardless of the starting values of the classes whenever $\tilde{R}_o^{CV} > 1$.

3.3. Analysis of the COVID-19-TB co-infection model

3.3.1. Disease-free equilibrium and reproduction of the co-infection model

The disease-free equilibrium of the COVID-19-TB co-infection model (2.12) is given by

$$\begin{aligned} E_F^o &= (S^o, L_T^o, I_T^o, L_C^o, I_C^o, L_{TC}^o, I_{TC}^o, T^o, V^o, R^o) \\ &= \left(\frac{(1-(a+b))\Lambda}{\mu}, 0, 0, 0, 0, 0, 0, 0, \frac{(a+b)\Lambda}{\mu}, 0\right). \end{aligned} \tag{3.38}$$

Then, using the next-generation matrix method as in [50], the associated reproduction number is given by

$$R_o^F = \frac{(1-a-b)(B + \sqrt{A})}{2K_6 K_4 K_3 K_2 K_1}, \tag{3.39}$$

where

$$\begin{aligned} A &= {\beta_1}^2\alpha^2\,{K_4}^2{K_3}^2\,(m\theta+K_6)^2 \\ &\quad -2\beta_1\beta_2\psi\alpha K_4\,K_1\,K_2K_3\left({K_6}^2+(m\theta+n\upsilon)\,K_6-n\theta\,m\upsilon\right) \\ &\quad +{\beta_2}^2\psi^2{K_1}^2{K_2}^2\,(n\upsilon+K_6)^2\,, \\ B &= \beta_2\psi\,K_2K_1(n\upsilon+K_6)+\beta_1\alpha\,K_4K_3(m\theta+K_6) \end{aligned} \tag{3.40}$$

and

$$\begin{aligned} &K_1=\mu+\alpha,\quad K_2=\mu+\delta_T+\gamma+\theta,\quad K_3=\mu+\psi+\chi, \\ &K_4=\mu+\delta_C+\upsilon+\varphi,\quad K_6=\mu+\delta_{TC}+\tau. \end{aligned} \tag{3.41}$$

Hence, given Theorem 2 of [51,53], we claim the following result:

Lemma 3.3. *The disease-free equilibrium E_F^o of the COVID-19-TB-model* (2.12) *is locally asymptotically stable if $R_o^F<1$, but not if $R_o^F>1$.*

The epidemiological interpretation of Figure 2 indicates that the disease may dies out in the population regards of the initial size. The following Theorem 3.3 confirms the disease free equilibrium in the case $\mathcal{R}_0^{CV}<1$, while that of Figure 3 shows that the disease may keep persistent in the population irrespective of the initial size of the infected individual. The following Theorem 3.4 affirms the persistence of the disease in the case $\tilde{\mathcal{R}}_0^{CV}>1$.

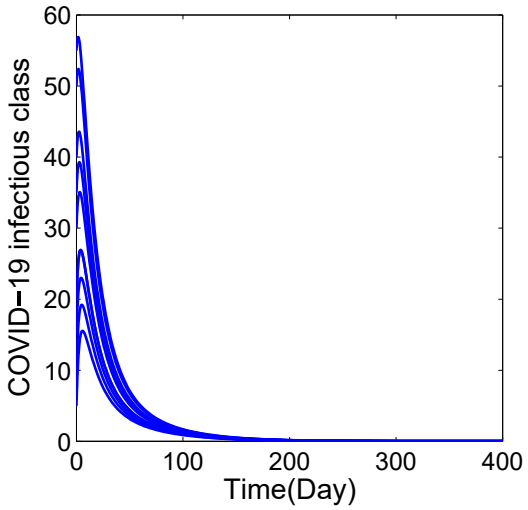

Figure 2. Simulation showing global stability of disease-free equilibrium points of infectious COVID-19 population equilibrium with various initial values and the parameter values as presented in Table 2, except that $\beta_2=0.19$ when $\mathcal{R}_0^{CV}=0.7350$.

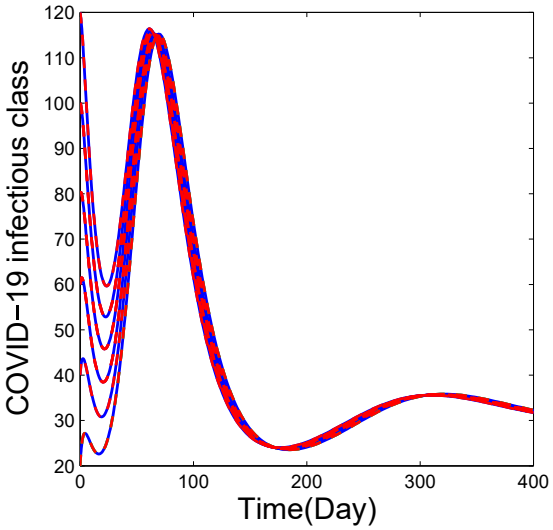

Figure 3. Simulation showing global stability of endemic equilibrium points of infectious COVID-19 population with various initial values and the parameter values as presented in Table 2, except that $\beta_2=0.69$ when $\tilde{\mathcal{R}}_0^{CV}>1$.

3.3.2. Global stability of disease-free equilibrium of COVID-19-TB co-infection model

Using the method presented by Castillo-Chavez et al. [50], we can write the model (2.12) as follows:

$$\begin{cases} \dfrac{dP}{dt}=A(P,I), \\ \dfrac{dI}{dt}=B(P,I), \qquad B(P,0)=0. \end{cases} \tag{3.42}$$

Then, the global asymptotic stability of the disease-free equilibrium is guaranteed if the following conditions hold:

Y1. For $\dfrac{dP}{dt}=A(P,0)$, P^* is globally asymptotically stable;

Y2. $B(P,I)=HI-\tilde{B}(P,I)\geq 0$ for $(P,I)\in D$,

where

$$H=D_IB(P^*,0)$$

is an M-matrix (the off-diagonal elements of H are non-negative) and D is the feasible region in which the model makes sense.

Theorem 3.5. *If the disease-free equilibrium E_F^o of the COVID-19-TB co-infection model* (2.12) *is locally asymptotically stable, then, it is also globally asymptotically stable if the conditions* (*Y*1) *and* (*Y*2) *are satisfied.*

Proof. For model (2.12),

$$P = (S, V, R)$$

and

$$I = (L_T, I_T, L_C, I_C, L_{TC}, I_{TC}, T).$$

$$A(P,0) = \begin{bmatrix} [1-(a+b)]\Lambda - \mu S \\ (a+b)\Lambda - \mu V \\ 0 \end{bmatrix}, \tag{3.43}$$

$$H = \begin{pmatrix} -K_1 & \beta_1[1-(a+b)] & 0 & 0 & 0 & \beta_1 m[1-(a+b)] & 0 \\ \alpha & -K_2 & 0 & 0 & 0 & 0 & 0 \\ 0 & 0 & -K_3 & \beta_2[1-(a+b)] & 0 & \beta_2 n[1-(a+b)] & 0 \\ 0 & 0 & \psi & -K_4 & 0 & 0 & 0 \\ 0 & 0 & 0 & 0 & -K_5 & 0 & 0 \\ 0 & \theta & 0 & \upsilon & \rho & -K_6 & 0 \\ 0 & \gamma & 0 & \varphi & 0 & \tau & -K_7 \end{pmatrix}, \tag{3.44}$$

where $K_5 = \mu + \rho$, $K_7 = \phi + \mu$, and K_1, K_2, K_3K_4, K_6 have been defined in (3.41).

Then,

$$\tilde{B}(P,I) = \begin{bmatrix} \beta_1(I_T + mI_{TC})\left[[1-(a+b)] - \dfrac{S}{N}\right] + \dfrac{\eta\beta_2 L_T(I_C + nI_{TC})}{N} \\ 0 \\ \beta_2(I_C + nI_{TC})\left[[1-(a+b)] - \dfrac{S}{N}\right] + \dfrac{\varepsilon\beta_1 L_C(I_T + mI_{TC})}{N} \\ 0 \\ -\dfrac{\eta L_T\beta_2(I_C + nI_{TC})}{N} - \dfrac{\varepsilon L_C\beta_1(I_T + mI_{TC})}{N} \\ 0 \\ 0 \end{bmatrix}. \tag{3.45}$$

From (3.45), $\tilde{B}_5(P,I) < 0$, which means that (Y2) is not satisfied. Hence, the disease-free equilibrium E_F^o may not be globally asymptotically stable. This implies that multiple endemic equilibria may exist; thus, we decided to investigate the possibility of backward bifurcation. □

3.3.3. Bifurcation analysis of the COVID-19-TB co-infection model

The approach presented by Castillo-Chavez and Song [54] is adopted to determine the type of bifurcation in the co-infection model. The method used was derived from the centre manifold theory. Now, we can establish the following result:

Theorem 3.6. *The model* (2.12) *exhibits backward bifurcation at* $R_o^F = 1$ *if* $a > 0$ *when* $R_o^F < 1$*; otherwise, it exhibits forward bifurcation, where*

$$\begin{aligned} a = \frac{2\mu}{\Lambda}\Big(& [\beta_1^* v_2(mw_7 + w_3) + \beta_2 v_4(nw_7 + w_5)][w_1(a+b) \\ & - (1-(a+b))(w_2 + w_3 + w_5 + w_7 + w_8 + w_{10})] \\ & + \beta_1^* v_2(mw_7 + w_3)[v_6(\varepsilon w_4 + \eta w_2) - (\eta v_2 w_2 + \varepsilon v_4 w_4)]\Big). \end{aligned}$$

Proof. The approach of Castillo-Chavez and Song [54] will be followed. We start by changing the variables as follows:

$$S = x_1, L_T = x_2, I_T = x_3, L_C = x_4, I_C = x_5,$$
$$L_{TC} = x_6, I_{TC} = x_7, T = x_8, V = x_9, R = x_{10}$$

and establishing that

$$N = x_1 + x_2 + x_3 + x_4 + x_5 + x_6 + x_7 + x_8 + x_9 + x_{10}.$$

So, if we use the vector form

$$X = (x_1, x_2, x_3, x_4, x_5, x_6, x_7, x_8, x_9, x_{10})^T,$$

then the model (2.12) is represented as follows:

$$\frac{dX}{dt} = (f_1, f_2, f_3, f_4, f_5, f_6, f_7, f_8, f_9, f_{10})^T.$$

Thus, model (2.12) becomes

$$\begin{cases} \dfrac{dx_1}{dt} = (1-(a+b))\Lambda - \lambda_T x_1 - \lambda_C x_1 - \mu x_1 = f_1, \\ \dfrac{dx_2}{dt} = \lambda_T x_1 - (\mu + \alpha + \eta\lambda_C)x_2 = f_2, \\ \dfrac{dx_3}{dt} = \alpha x_2 - (\mu + \delta_T + \gamma + \theta)x_3 = f_3, \\ \dfrac{dx_4}{dt} = \lambda_C x_1 - (\mu + \chi + \varepsilon\lambda_T + \psi)x_4 = f_4, \\ \dfrac{dx_5}{dt} = \psi x_4 - (\mu + \delta_C + \upsilon + \varphi)x_5 = f_5, \\ \dfrac{dx_6}{dt} = \eta\lambda_C x_2 + \varepsilon\lambda_T x_4 - (\mu + \rho)x_6 = f_6, \\ \dfrac{dx_7}{dt} = \rho x_6 + \theta x_3 + \upsilon x_5 - (\mu + \delta_{TC} + \tau)x_7 = f_7, \\ \dfrac{dx_8}{dt} = \gamma x_3 + \varphi x_5 + \tau x_7 - (\phi + \mu)x_8 = f_8, \\ \dfrac{dx_9}{dt} = a\Lambda + b\Lambda - \mu x_9 = f_9, \\ \dfrac{dx_{10}}{dt} = \phi x_8 + \chi x_4 - \mu x_{10} = f_{10}, \end{cases} \tag{3.46}$$

where

$$\lambda_T = \frac{\beta_1(x_3 + mx_7)}{x_1 + x_2 + x_3 + x_4 + x_5 + x_6 + x_7 + x_8 + x_9 + x_{10}},$$
$$\lambda_C = \frac{\beta_2(x_5 + nx_7)}{x_1 + x_2 + x_3 + x_4 + x_5 + x_6 + x_7 + x_8 + x_9 + x_{10}}.$$

If β_1 is taken as the bifurcation parameter at $R_o^F = 1$, then

$$\begin{aligned}\beta_1 &= \beta_1^* \\ &= \frac{K_2K_1[K_6K_4K_3 - \beta_2\psi\ (1-a-b)\,(n\upsilon + K_6)\,]}{\left(\begin{array}{l}\alpha\ (1-a-b)\,[K_3K_4\,(m\theta + K_6) \\ -\beta_2\psi\ (m\theta + n\upsilon + K_6)\,(1-a-b)\,]\end{array}\right)}.\end{aligned} \tag{3.47}$$

The Jacobian of (3.46), evaluated at E_F^o, is denoted by $J(E_F^o)$; also by adopting the method in [54, 55], the Jacobian $J(E_F^o)$ has right and left eigenvectors w and v that correspond to the simple zero eigenvalue such that $w.v = 1$. The right eigenvector is given by

$$w = (w_1, w_2, w_3, w_4, w_5, w_6, w_7, w_8, w_9, w_{10})^T, \tag{3.48}$$

where

$$\begin{aligned}w_1 &= \frac{-[1-(a+b)]\Big[\beta_1^*[w_3 + mw_7] + \beta_2[w_5 + nw_7]\Big]}{\mu}, \\ w_6 = 0,\ \ w_2 &= \frac{\beta_1^*[1-(a+b)]\Big[w_3 + mw_7\Big]}{K_1},\ \ w_7 = w_7 > 0, \\ w_3 = w_3 > 0,\ \ w_8 &= \frac{\gamma w_3 + \varphi w_5 + \tau w_7}{K_7},\ \ w_9 = 0, \\ w_4 &= \frac{\beta_2[1-(a+b)]\Big[w_5 + nw_7\Big]}{K_3},\ \ w_{10} = \frac{\theta w_8 + \chi w_4}{\mu}, \\ w_5 &= w_5 > 0.\end{aligned}$$

The left eigenvector v is given by

$$v = (v_1, v_2, v_3, v_4, v_5, v_6, v_7, v_8, v_9, v_{10}),$$

where

$$\begin{aligned}v_1 = 0,\ \ v_6 &= \frac{\rho v_7}{K_5},\ \ v_2 = v_3 > 0, \\ v_7 &= \frac{[1-(a+b)](\beta_1^* m v_2 + \beta_2 n v_4)}{K_4}, \\ v_3 &= \frac{\theta v_7 + \beta_1^* v_2[1-(a+b)]}{K_2}, \\ v_8 = 0,\ \ v_4 &= v_4 > 0, v_9 = 0, \\ v_5 &= \frac{\upsilon v_7 + \beta_2 v_4[1-(a+b)]}{K_4},\ \ v_{10} = 0.\end{aligned}$$

where $K_5 = \mu + \rho, K_7 = \phi + \mu$ and K_1, K_2, K_3K_4, K_6, have been defined in (3.41).

We then compute the bifurcation coefficients a and b, defined as follows:

$$a = \sum_{k,i,j=1}^{n} v_k w_i w_j \frac{\partial^2 f_k}{\partial x_i \partial x_j}(0,0),$$

$$b = \sum_{k,i=1}^{n} v_k w_i \frac{\partial^2 f_k}{\partial x_i \partial \beta_1^*}(0,0).$$

Thus,

$$\begin{aligned}a = \frac{2\mu}{\Lambda}\Big([\beta_1^* v_2(mw_7 + w_3) + \beta_2 v_4(nw_7 + w_5)][w_1(a+b) \\ -(1-(a+b))(w_2 + w_3 + w_5 + w_7 + w_8 + w_{10})] \\ +\beta_1^* v_2(mw_7 + w_3)[v_6(\varepsilon w_4 + \eta w_2) - (\eta v_2 w_2 + \varepsilon v_4 w_4)]\Big)\end{aligned} \tag{3.49}$$

and

$$b = v_2(1-(a+b))\Big[w_3 + mw_7\Big]. \tag{3.50}$$

From (3.50), $b > 0$; consequently, from Theorem 3.6, the COVID-19-TB co-infection model will exhibit backward bifurcation if a in (3.49) is positive. The parameters that lead to the backward bifurcation observed in the co-infection model when $R_o^F < 1$ are η, i.e., rate at which latent TB individuals become latently infected with COVID-19, and ε, i.e., rate at which latent COVID-19 individuals become latently infected with TB. □

This means that the classical condition $R_o^F < 1$ required for the elimination of the co-infection is necessary but not sufficient to guarantee adequate control of COVID-19-TB co-infection. This implies that it will be difficult to manage COVID-19-TB co-infection. Figure 4 is a diagrammatic representation of the contents of Subsection 3.3.3.

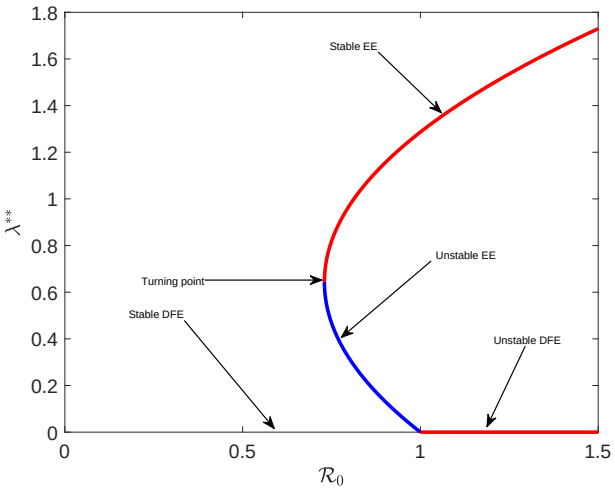

Figure 4. Simulation showing backward bifurcation.

3.4. Uncertainty and sensitivity analysis

As a result the model (2.12) comprising many parameters, uncertainty will arise. To ascertain the impact of different parameters of the model, uncertainty and sensitivity analysis was performed by using Latin hypercube sampling (LHS) and the partial rank correlation coefficient (PRCC). LHS was used to sample the 17 parameters required to determine the reproduction number R_o^F, and the PRCC was used for the global sensitivity analysis of R_o^F. For more details on this method, see [56–58]. The significance of this analysis is that it helps to identify the parameters that contribute massively to the spread and control of the co-infection [59]. The signs of the PRCCs indicate the relationship between the response function R_o^F and the parameters. It is important to note that this analysis helps to predict the necessary policy measures. The parameters with negative PRCCs show that they are negatively correlated, and parameters with positive PRCCs indicate that they are positively correlated. If the absolute value of a PRCC of a parameter is greater than or equal to 0.5, then such a parameter is statistically important. The results of the computed PRCCs are given in Table 3.

Table 3. The values of the PRCCs

Parameter	PRCC	Parameter	PRCC
υ	0.15957	μ	-0.00089
m	0.16899	n	0.41851
γ	-0.05719	β_1	0.06647
β_2	0.87130	τ	-0.06119
α	-0.01836	ψ	0.01265
χ	-0.00265	φ	-0.20452
θ	-0.01220	δ_T	-0.00526
δ_C	-0.74791	δ_{TC}	-0.46910
a	-0.52019	b	-0.56013

4. Results and discussion

Various simulation experiments were carried out by employing ODE45 in Matlab with the parameter values in Table 2; the results are presented in Figures 2–12.

The parameter values used were obtained from the literature, with the references stated in Table 2. It should be noted that the initial data of the sub-populations used were hypothetical values. Figure 2 shows to us the possibilities of eliminating COVID-19 in the population regardless of the initial size of infected individual provided that $\mathcal{R}_0^{CV} < 1$. on the other-hands, if $\tilde{\mathcal{R}}_0^{CV} > 1$ the diseases will persist in the population, this is clearly shown in Figure 3. Figure 4 shows the co-existence of the stable disease-free equilibrium and endemic equilibrium. Thus, The classical condition $R_o^F < 1$ required for the elimination of the co-infection is necessary but not sufficient to guarantee adequate control of COVID-19-TB co-infection. Then, this will make it difficult to manage the COVID-19-TB co-infection.

The results of the uncertainty and sensitivity analysis using LHS/PRCC are given in Table 3, and the bar plot of the results is depicted in Figure 5. From the analysis, the most important parameters, i.e., with |PRCC| ≥ 0.5, are β_2, δ_C, b, and a, which are the rate of transmission of the COVID-19, death from COVID-19, the proportion vaccinated against the COVID-19, and the proportion vaccinated with BCG. β_2 was found to be positively correlated, which means that its increase will give rise to a corresponding increase in the value of R_o^F. Hence, non-pharmaceutical measures should be put in place to minimize the transmission rate β_2. However, a and b were found to be negatively correlated, which signifies that they have decreasing effects on R_o^F, when they are increased. Thus, increasing the proportion of people vaccinated against COVID-19 and TB can also control the incidence of the COVID-19-TB co-infection. Hence, interventions that can help to increase the vaccinated proportion should be considered (e.g., adequate funding and manpower, use of media, community engagement, and improved access to vaccine).

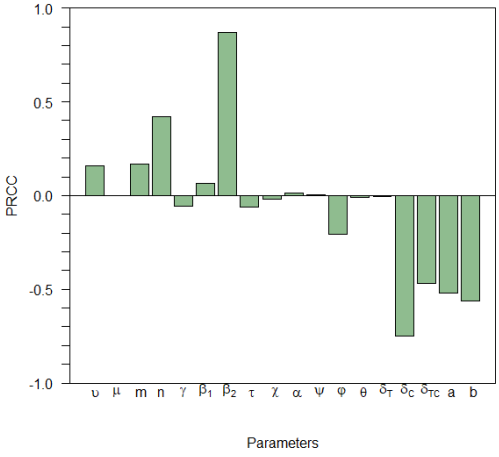

Figure 5. Bar plot of the PRCCs.

Figure 6 presents the contour graph to illustrate the impact of a and b on the reproduction number R_o^F of the complete model. The associated reproduction number R_o^F increases as the proportions a and b of vaccinated people decrease; this is consistent with the results of the sensitivity analysis. Figure 7 indicates that, with a low transmission rate of COVID-19 infection, the proportion of people required to be vaccinated with BCG and against COVID-19 to have the reproduction number R_o^F be less than unity will be small. The illustration in Figure 8 depicts the effects of the COVID-19 transmission rate and vaccination proportions a and b on the associated reproduction number R_o^F. It is observed that lowering the transmission rate and increasing the proportions a and b reduce the reproduction number R_o^F. This means that a smaller number of people will be co-infected with the COVID-19-TB if the proportions of people vaccinated with BCG and against COVID-19 are large and there is a reduced COVID-19 transmission rate.

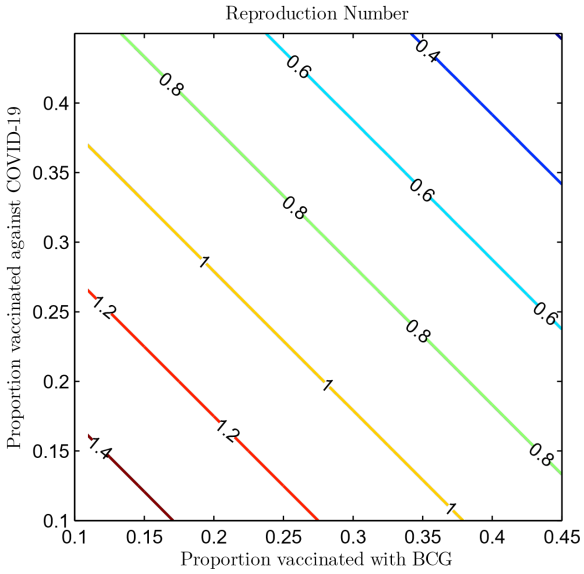

Figure 6. Contour graph of the associated reproduction number of the co-infection as functions of a and b.

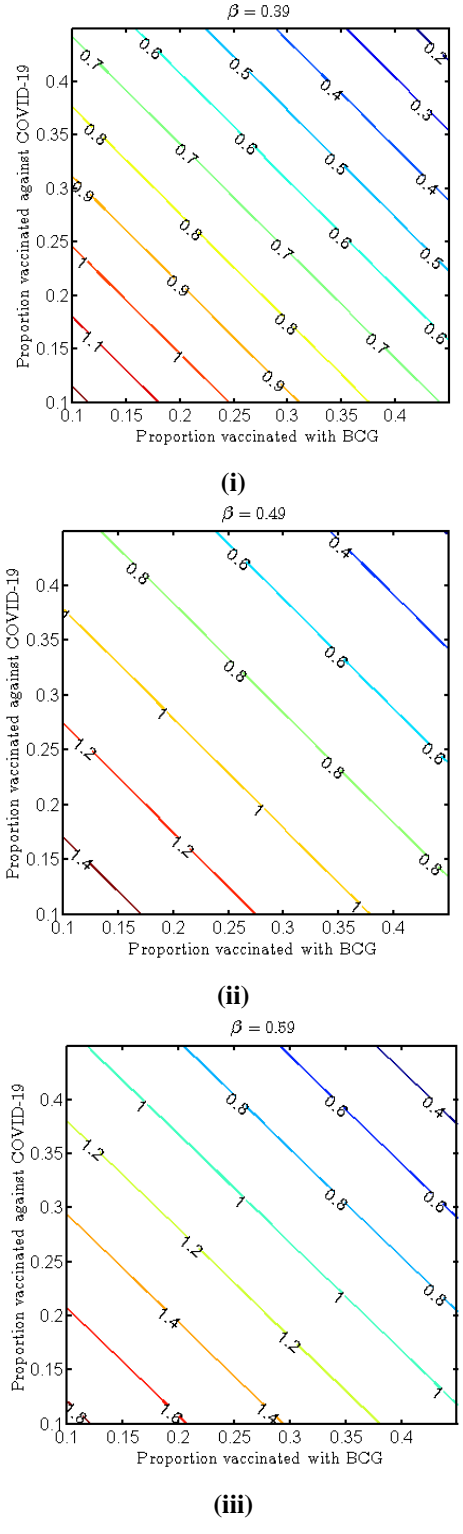

Figure 7. Contour graph of the associated reproduction number of the co-infection as functions of a and b with different transmission rates β_2.

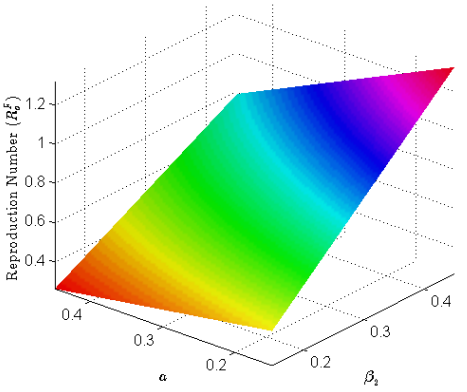

(i)

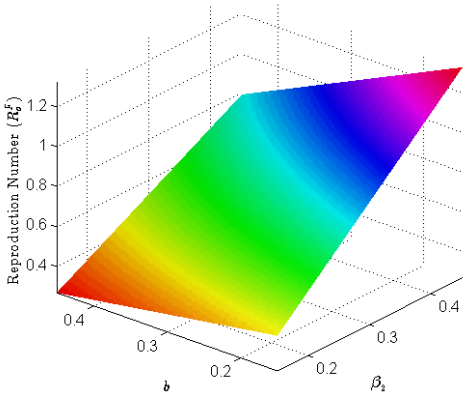

(ii)

Figure 8. 3D plots illustrating the effects of transmission rate β_2 of COVID-19 and vaccinated proportions a and b on the associated reproduction number of the co-infection model.

The long-term dynamics of the infectious COVID-19-TB co-infected population depicted in Figure 9 indicate that co-infection will persist in the population whenever $R_o^F > 1$. Moreover, the effect of the rate of transmission of COVID-19 is illustrated in Figure 10. The infectious population of the co-infected individuals was found to reach the highest peak within a very short time under the maximum transmission rate. Hence, the large number of infectious COVID-19-TB co-infected populations that is subject to a high transmission rate of COVID-19 should be addressed by implementing interventions that can reduce the transmission rate.

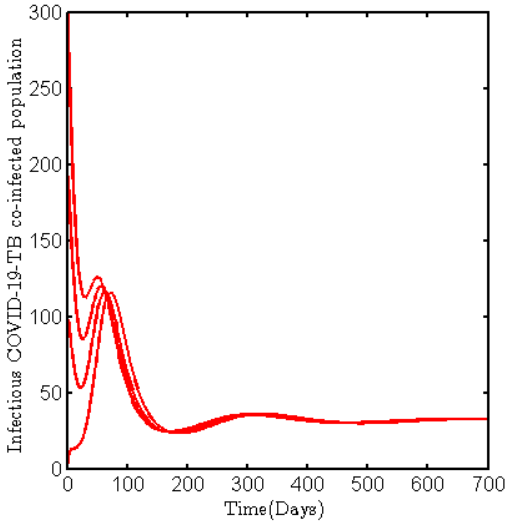

Figure 9. Long-term dynamics of the infectious COVID-19-TB co-infected population with $\beta_2 = 0.69$ when $R_o^F > 1$.

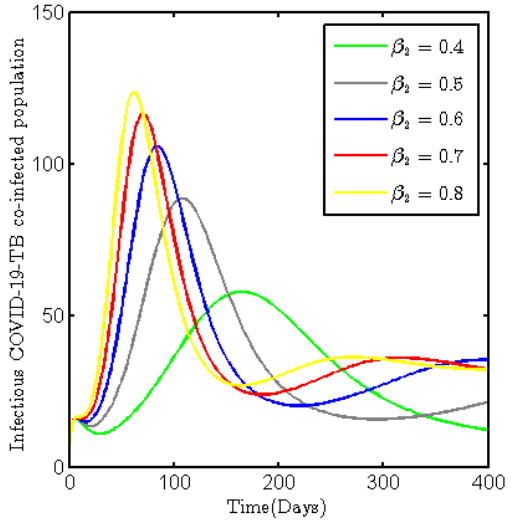

Figure 10. Plot of the infectious COVID-19-TB co-infected population against time for various transmission rates β_2.

Furthermore, the solution lines of infectious COVID-19-TB co-infected population when the proportions a and b were varied simultaneously are depicted in Figure 11. The population declines as these proportions increase, and this is related to the interpretation of the sensitivity analysis results. The plot in the Figure 12 shows the infectious COVID-19-TB co-infected population when the transmission rate β_2

is varied with different values of a and b. A decrease in population size was observed, and it is attributed to the increase in the proportions a and b of vaccinated people. Hence, interventions that can reduce the rate of transmission of COVID-19 and interventions targeted at increasing the proportion of people vaccinated should be concurrently considered to mitigate the burden of the co-infection.

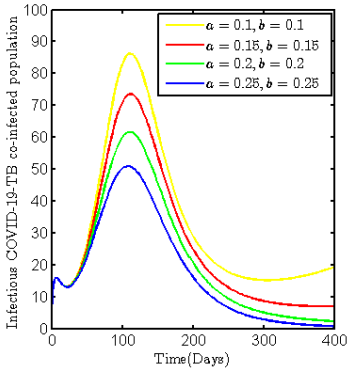

Figure 11. Plot of the infectious COVID-19-TB co-infected population against time for varying proportions a and b.

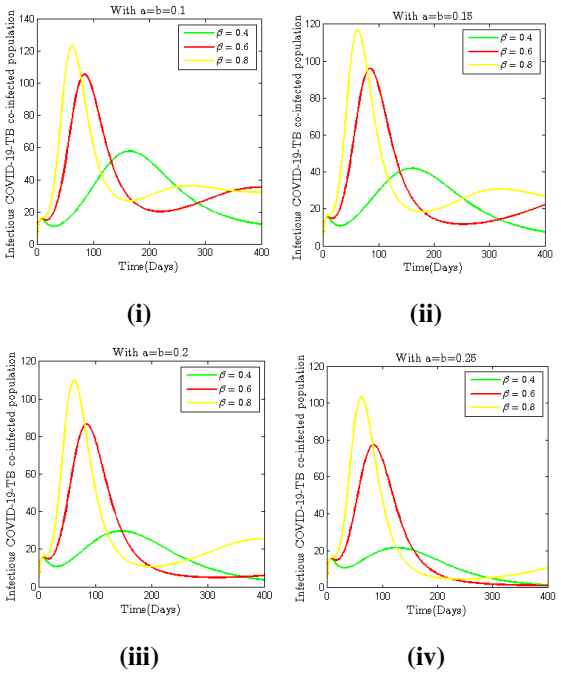

Figure 12. Plot of the infectious COVID-19-TB co-infected population against time for various transmission rates β_2 different values of a and b.

5. Conclusions

A mathematical model of the dynamics of COVID-19-TB co-infection has been presented and studied. The disease-free and endemic equilibria of the two sub-models have been obtained and found to be globally asymptotically stable when their control reproduction numbers $R_o^{TV}, R_o^{CV} < 1$ and $\tilde{R}_o^{TV}, \tilde{R}_o^{CV} > 1$, respectively. However, the co-infection model was found to exhibit backward bifurcation. Furthermore, uncertainty and sensitivity analysis was performed by using LHS and the PRCC to determine the impact of different parameters of the model. The simulation results suggest that a reduction in the rate of transmission and an increment in the proportions of people vaccinated with BCG and against TB can lower the number of COVID-19 cases. Therefore, interventions aimed at reducing the transmission rate and increasing the proportion of people vaccinated against TB and COVID-19, such as the use of face masks, good sanitation practices, massive vaccination funding, programs, and campaigns, should be prioritized. Based on the limitations stated earlier, we wish to explore the fractional order of the model and use real data to simulate and predict the dynamics of the model in our future research.

Use of AI tools declaration

The authors declare they have not used Artificial Intelligence (AI) tools in the creation of this article.

Conflict of interest

Authors declare no conflicts of interest.

References

1. World Health Organization, Coronavirus disease (COVID-19), 2023. Available from: https://www.who.int/news-room/fact-sheets/detail/coronavirus-disease-(covid-19).
2. COVID-19, 2020. Available from: https://www.cdc.gov/coronavirus/2019-ncov/your-health/about-covid-19.html.
3. Tuberculosis (TB)-basic TB facts, 2019. Available from: https://www.cdc.gov/tb/topic/basics/default.html.

4. World Health Organization, Tuberculosis and COVID- 19, 2020. Available from: https://www.who.int/teams/global-tuberculosis-programme/covid-19.
5. H. Yang, S. Lu, COVID-19 and tuberculosis, *J. Transl. Int. Med.*, **8** (2020), 59–65. https://doi.org/10.2478/jtim-2020-0010
6. G. T. Mousquer, A. Peres, M. Fiegenbaum, Pathology of TB/COVID-19 co-infection: the phantom menace, *Tuberculosis*, **126** (2021), 102020. https://doi.org/10.1016/j.tube.2020.102020
7. B. Diao, C. Wang, Y. Tan, X. Chen, Y. Liu, L. Ning, et al., Reduction and functional exhaustion of T cells in patients with coronavirus disease 2019 (COVID-19), *Front. Immunol.*, **11** (2020), 827. https://doi.org/10.3389/fimmu.2020.00827
8. M. Khayat, H. Fan, Y. Vali, COVID-19 promoting the development of active tuberculosis in a patient with latent tuberculosis infection: a case report, *Respir. Med. Case Rep.*, **32** (2021), 101344. https://doi.org/10.1016/j.rmcr.2021.101344
9. M. Tadolini, L. R. Codecasa, J. M. García-García, F. X. Blanc, S. Borisov, J. W. Alffenaar, et al., Active tuberculosis, sequelae and COVID-19 co-infection: first cohort of 49 cases, *Eur. Respir. J.*, **56** (2020), 2001398. https://doi.org/10.1183/13993003.01398-2020
10. A. Abdoli, S. Falahi, A. Kenarkoohi, COVID-19-associated opportunistic infections: a snapshot on the current reports, *Clin. Exp. Med.*, **22** (2022), 327–346. https://doi.org/10.1007/s10238-021-00751-7
11. M. Kretzschmar, Disease modeling for public health: added value, challenges, and institutional constraints, *J. Public Health Policy*, **41** (2020), 39–51. https://doi.org/10.1057/s41271-019-00206-0
12. Y. Wu, M. Huang, X. Wang, Y. Li, L. Jiang, Y. Yuan, The prevention and control of tuberculosis: an analysis based on a tuberculosis dynamic model derived from the cases of Americans, *BMC Publ. Health*, **20** (2020), 1173. https://doi.org/10.1186/s12889-020-09260-w
13. L. N. Nkamba, T. T. Manga, F. Agouanet, M. L. Mann Manyombe, Mathematical model to assess vaccination and effective contact rate impact in the spread of tuberculosis, *J. Biol. Dyn.*, **13** (2019), 26–42. https://doi.org/10.1080/17513758.2018.1563218
14. S. Liu, Y. Bi, Y. Liu, Modeling and dynamic analysis of tuberculosis in mainland China from 1998 to 2017: the effect of DOTS strategy and further control, *Theor. Biol. Med. Modell.*, **2020** (2020), 17. https://doi.org/10.1186/s12976-020-00124-9
15. K. C. Chong, C. C. Leung, W. W. Yew, B. C. Y. Zee, G. C. H. Tam, M. H. Wang, et al., Mathematical modelling of the impact of treating latent tuberculosis infection in the elderly in a city with intermediate tuberculosis burden. *Sci. Rep.*, **9** (2019), 4869. https://doi.org/10.1038/s41598-019-41256-4
16. T. A. Perkins, G. España, Optimal control of the COVID-19 pandemic with non-pharmaceutical interventions, *Bull. Math. Biol.*, **82** (2020), 118. https://doi.org/10.1007/s11538-020-00795-y
17. S. I. Oke, M. I. Ekum, O. J. Akintande, M. O. Adeniyi, T. A. Adekiya, O. J. Achadu, et al., Optimal control of the coronavirus pandemic with both pharmaceutical and non-pharmaceutical interventions, *Int. J. Dyn. Control*, **11** (2023), 2295–2319. https://doi.org/10.1007/s40435-022-01112-2
18. M. Zamir, F. Nadeem, M. A. Alqudah, T. Abdeljawad, Future implications of COVID-19 through mathematical modeling, *Results Phys.*, **33** (2022), 105097. https://doi.org/10.1016/j.rinp.2021.105097
19. L. Masandawa, S. S. Mirau, I. S. Mbalawata, Mathematical modeling of COVID-19 transmission dynamics between healthcare workers and community, *Results Phys.*, **29** (2021), 104731. https://doi.org/10.1016/j.rinp.2021.104731
20. A. O. Atede, A. Omame, S. C. Inyama, A fractional order vaccination model for COVID-19 incorporating environmental transmission: a case study using Nigerian data, *Bull. Biomath.*, **1** (2023), 78–110. https://doi.org/10.59292/bulletinbiomath.2023005
21. B. Yang, Z. Yu, Y. Cai, The impact of vaccination on the spread of COVID-19: studying by a mathematical model, *Phys. A*, **590** (2022), 12671. https://doi.org/10.1016/j.physa.2021.126717

22. A. Kouidere, O. Balatif, M. Rachik, Cost-effectiveness of a mathematical modeling with optimal control approach of spread of COVID-19 pandemic: a case study in Peru, *Chaos Solitons Fract.*, **10** (2023), 100090. https://doi.org/10.1016/j.csfx.2022.100090

23. C. N. Ngonghala, E. Iboi, S. Eikenberry, M. Scotch, C. R. MacIntyre, M. H. Bonds, et al., Mathematical assessment of the impact of non-pharmaceutical interventions on curtailing the 2019 novel Coronavirus, *Math. Biosci.*, **325** (2020), 108364. https://doi.org/10.1016/j.mbs.2020.108364

24. O. Sharomi, C. N. Podder, A. B. Gumel, B. Song, Mathematical analysis of the transmission dynamics of HIV/TB coinfection in the presence of treatment, *Math. Biosci. Eng.*, **5** (2008), 145–174. https://doi.org/10.3934/mbe.2008.5.145

25. Z. Mukandavire, A. B. Gumel, W. Garira, J. M. Tchuenche, Mathematical analysis of a model for HIV-malaria co-infection, *Math. Biosci. Eng.*, **6** (2009), 333–362. https://doi.org/10.3934/mbe.2009.6.333

26. H. T. Alemneh, A co-infection model of dengue and leptospirosis diseases, *Adv. Differ. Equations*, **2020** (2020), 664. https://doi.org/10.1186/s13662-020-03126-6

27. I. M. Hezam, A. Foul, A. Alrasheedi, A dynamic optimal control model for COVID-19 and cholera co-infection in Yemen, *Adv. Differ. Equations*, **2021** (2021), 108. htttps://doi.org/10.1186/s13662-021-03271-6

28. V. Guseva, N. Doktorova, O. Krivorotko, O. Otpushchennikova, L. Parolina, I. Vasilyeva, et al., Building a seir-model for predicting the HIV/tuberculosis coinfection epidemic for russian territories with low TB burden, *Int. J. Infect. Dis.*, **134** (2023), S4-S5. https://doi.org/10.1016/j.ijid.2023.05.028

29. A. Ahmad, M. Farman, A. Akgül, N. Bukhari, S. Imtiaz, Mathematical analysis and numerical simulation of co-infection of TB-HIV, *Arab J. Basic Appl. Sci.*, **27** (2020), 431–441. https://doi.org/10.1080/25765299.2020.1840771

30. A. Omame, A. D. Okuonghae, U. E. Nwafor, B. U. Odionyenma, A co-infection model for HPV and syphilis with optimal control and cost-effectiveness analysis, *Int. J. Biomath.*, **14** (2021), 2150050. https://doi.org/10.1142/S1793524521500509

31. A. Omame, M. Abbas, C. P. Onyenegecha, A fractional-order model for COVID-19 and tuberculosis co-infection using Atangana-Baleanu derivative, *Chaos Solitons Fract.*, **153** (2021), 111486. https://doi.org/10.1016/j.chaos.2021.111486

32. A. Omame, M. Abbas, C. P. Onyenegecha, A fractional order model for the co-interaction of COVID-19 and Hepatitis B virus, *Results Phys.*, **37** (2022), 105498. https://doi.org/10.1016/j.rinp.2022.105498

33. H. Rwezaura, M. L. Diagne, A. Omame, A. L. de Espindola, J. M. Tchuenche, Mathematical modeling and optimal control of SARS-CoV-2 and tuberculosis co-infection: a case study of Indonesia, *Model. Earth Syst. Environ.*, **8** (2022), 5493–5520. https://doi.org/10.1007/s40808-022-01430-6

34. R. I. Gweryina, C. E. Madubueze, V. P. Bajiya, F. E. Esla, Modeling and analysis of tuberculosis and pneumonia co-infection dynamics with cost-effective strategies, *Results Control Optim.*, **10** (2023), 100210. https://doi.org/10.1016/j.rico.2023.100210

35. K. G. Mekonen, L. L. Obsu, Mathematical modeling and analysis for the co-infection of COVID-19 and tubercu-losis, *Heliyon*, **8** (2022), e11195. https://doi.org/10.1016/j.heliyon.2022.e11195

36. K. G. Mekonen, S. F. Balcha, L. L. Obsu, A. Hassen, Mathematical modeling and analysis of TB and COVID-19 coinfection, *J. Appl. Math.*, **2022** (2022), 2449710. https://doi.org/10.1155/2022/2449710

37. A. Selvam, S. Sabarinathan, B. V. S. Kumar, H. Byeon, K. Guedri, S. M. Eldin, et al., Ulam-Hyers stability of tuberculosis and COVID-19 co-infection model under Atangana-Baleanu fractal-fractional operator, *Sci. Rep.*, **13** (2023), 9012. https://doi.org/10.1038/s41598-023-35624-4

38. S. R. Bandekar, M. Ghosh, A co-infection model on TB- COVID-19 with optimal control and sensitivity analysis, *Math. Comput. Simul.*, **200** (2022), 1–31. https://doi.org/10.1016/j.matcom.2022.04.001

39. F. Inayaturohmat, N. Anggriani, A. K. Supriatna, A mathematical model of tuberculosis and COVID-19 coinfection with the effect of isolation and treatment, *Front. Appl. Math. Stat.*, **8** (2022), 958081. htttps://doi.org/10.3389/fams.2022.958081

40. Z. S. Kifle, L. L. Obsu, Co-dynamics of COVID-19 and TB with COVID-19 vaccination and exogenous reinfection for TB: an optimal control application, *Infect. Dis. Modell.*, **8** (2023), 574–602. https://doi.org/10.1016/j.idm.2023.05.005

41. S. W. Teklu, Y. F. Abebaw, B. B. Terefe, D. K. Mamo, HIV/AIDS and TB co-infection deterministic model bifurcation and optimal control analysis, *Inf. Med. Unlocked*, **41** (2023), 101328. https://doi.org/10.1016/j.imu.2023.101328

42. B. S. Kotola, S. W. Teklu, Y. F. Abebaw, Bifurcation and optimal control analysis of HIV/AIDS and COVID-19 co-infection model with numerical simulation, *PLoS One*, **18** (2023), e0284759. https://doi.org/10.1371/journal.pone.0284759

43. S. W. Teklu, Mathematical analysis of the transmission dynamics of COVID-19 infection in the presence of intervention strategies, *J. Biol. Dyn.*, **16** (2022), 640–664. https://doi.org/10.1080/17513758.2022.2111469

44. S. W. Teklu, B. B. Terefe, D. K. Mamo, Y. F. Abebaw, Optimal control strategies on HIV/AIDS and pneumonia co-infection with mathematical modelling approach, *J. Biol. Dyn.*, **18** (2024), 2288873. https://doi.org/10.1080/17513758.2023.2288873

45. D. Okuonghae, S. Omosigho, Analysis of a mathematical model for tuberculosis: what could be done to increase case detection, *J. Theor. Biol.*, **269** (2011), 31–45. https://doi.org/10.1016/j.jtbi.2010.09.044

46. S. M. Garba, J. M. S. Lubuma, B. Tsanou, Modeling the transmission dynamics of the COVID-19 pandemic in South Africa, *Math. Biosci.*, **328** (2020), 108441. https://doi.org/10.1016/j.mbs.2020.108441

47. S. A. Lauer, K. H. Grantz, Q. Bi, F. K. Jones, Q. Zheng, H. R. Meredith, et al., The incubation period of coronavirus disease 2019 (COVID-19) from publicly reported confirmed cases: estimation and application, *Ann. Int. Med.*, **172** (2020), 9. https://doi.org/10.7326/M20-0504

48. A. Alemu, Z. W. Bitew, G. Seid, G. Diriba, E. Gashu, N. Berhe, et al., Tuberculosis in individuals who recovered from COVID-19: a systematic review of case reports, *PLOS One*, **17** (2022), 0277807. https://doi.org/10.1371/journal.pone.0277807

49. D. Okuonghae, A. Omame, Analysis of a mathematical model for COVID-19 population dynamics in Lagos, Nigeria, *Chaos Solitons Fract.*, **139** (2020), 110032. https://doi.org/10.1016/j.chaos.2020.110032

50. C. Castillo-Chavez, Z. Feng, W. Huang, On the computation of R0 and its role in global stability, *Inst. Math. Appl.*, **125** (2002), 229.

51. P. van den Driessche, J. Watmough, Reproduction numbers and sub-threshold endemic equilibria for compartmental models of disease transmission, *Math. Biosci.*, **180** (2002), 29–48. https://doi.org/10.1016/s0025-5564(02)00108-6

52. J. P. LaSalle, *The stability of dynamical systems*, Society for Industrial and Applied Mathematics, 1976.

53. J. O. Akanni, A non-linear optimal control model for illicit drug use and terrorism dynamics in developing countries with time-dependent control variables, *Decis. Anal. J.*, **8** (2023), 100281. https://doi.org/10.1016/j.dajour.2023.100281

54. C. Castillo-Chavez, B. Song, Dynamical models of tuberculosis and their applications, *Math. Biosci. Eng.*, **1** (2004), 361–404. https://doi.org/10.3934/mbe.2004.1.361

55. A. Abidemi, J. O. Akanni, O. D. Makinde, A non-linear mathematical model for analysing the impact of COVID-19 disease on higher education in developing countries, *Healthcare Anal.*, **3** (2023), 100193. https://doi.org/10.1016/j.health.2023.100193

56. S. M. Blower, H. Dowlatabadi, Sensitivity and uncertainty analysis of complex models of disease transmission: an HIV model, as an example, *Int. Stat. Rev.*, **62** (1994), 229–243. https://doi.org/10.2307/1403510

57. M. A. Sanchez, S. M. Blower, Uncertainty and sensitivity analysis of the basic reproductive rate: tuberculosis as an example, *Amer. J. Epidemiol.*, **145** (1997), 1127–1137. https://doi.org/10.1093/oxfordjournals.aje.a009076

58. J. Wu, R. Dhingra, M. Gambhir, J. V. Remais, Sensitivity analysis of infectious disease models: methods, advances and their application, *J. R. Soc. Interface*, **10** (2013), 1018. https://doi.org/10.1098/rsif.2012.1018

59. S. Olaniyi, J. O. Akanni, O. A. Adepoju, Optimal control and cost-effectiveness analysis of an illicit drug use population dynamics, *J. Appl. Nonlinear Dyn.*, **12** (2023), 133–146. https://doi.org/10.5890/JAND.2023.03.010

AIMS Press